

Colloid-like scale-free cluster-cluster aggregation during polymer collapse

Suman Majumder[†]

Amity Institute of Applied Sciences, Amity University Uttar Pradesh, Noida 201313, India

Saikat Chakraborty^{*}

Laboratoire Interdisciplinaire de Physique, Université Grenoble Alpes, CNRS, 38402 Saint-Martin-d'Hères, France

An extended polymer collapses to form a globule when subjected to a quench below the collapse transition temperature. The process begins with the formation of clusters of monomers or “pearls”. The nascent clusters merge, resulting in growth of the average cluster size C_s , eventually leading to a single globule. The aggregation of the clusters are known to be analogous to droplet coalescence. This suggests a striking resemblance between such an aggregation and cluster-cluster aggregation in colloidal self-assembly, which is characterized by a universal dynamic scaling behavior. Motivated by that, here, we verify the presence of such dynamic scaling during the collapse of a polymer with varying bending stiffness κ , using molecular dynamic simulations. We probe the dynamics via time evolution of the size distribution of clusters $N_s(t)$ and growth of $C_s(t)$. Irrespective of κ , we observe the power-law scalings $C_s(t) \sim t^z$ and $N_s(t) \sim t^{-w}s^{-\tau}$, of which only the cluster growth is universal with $z \approx 1.65$. Importantly, our results indeed show that $N_s(t)$ exhibits a dynamic scaling of the form $N_s(t) \sim s^{-2}f(s/t^z)$, indicative of a scale-free cluster growth. Interestingly, for flexible and weakly stiff polymers the dynamic exponents obey the relation $w = 2z$, as also found in diffusion-controlled cluster-cluster aggregation of particles. For $\kappa \geq 5$, the exponents show deviation from this relation, which grows continuously with κ . We identify the differences in local structures of the clusters formed, leading to variations in cluster-size dependence of the effective diffusion constant to be the origin of the above deviation. We also discuss potential experimental strategies to directly visualize the observed dynamic scaling in a collapsing polymer.

I. INTRODUCTION

An extended polymer collapses to a globule when the monomer-monomer interaction overpowers the monomer-solvent interaction [1–3]. Typically, this is achieved via a quench below the associated collapse transition temperature or Θ -temperature. Following the quench, the polymer attains its equilibrium globular conformation through a nonequilibrium relaxation process [4–19]. Study of the nonequilibrium dynamics during the collapse have implications in understanding folding pathways of globular proteins [20–24]. In this context, recently it has been shown that intrinsically disordered proteins can have multiple stable structures akin to coil or globules [25, 26]. Conformational switch between two states may be mapped to a coil-globule transition in polymers. Thus, a deeper understanding of the nonequilibrium process is still of much fundamental interest.

The study of the collapse of a polymer can be traced back to the work of de Gennes [4]. It proposes the formation of dense “sausage” shaped conformations at early times through a uniform aggregation across the chain. Drive to minimize the interfacial free energy results in thickening of the sausage, eventually forming a spherical globule. Later studies suggest an alternate sequence of events, where dense regions along the polymer chain nucleate to form small clusters of monomers or “pearls”, giving rise to the so called “pearl-necklace” intermediate. Subsequently, these pearls grow further by acquiring monomers from adjacent segments of the polymer and at later they self aggregate upon collision forming a single cluster or

globule. This progression, proposed by Halperin and Goldbart [27] is slightly different from that of Klushin [10]. A chain-tension mediated merging of the clusters to final globule state is put forward in the latter’s work. Since monitoring a single polymer was difficult, experimental verification of this multi-stage collapse was rare in the past [12, 28], and hence most studies relied on computer simulations. Almost all of these studies confirmed the “pearl-necklace” as the phenomenological picture [19]. As a matter of fact, there are even evidences of observation of “pearl-necklace” in experiments as well [12]. However, recently it has been shown that depending on temperature and solvent viscosity the collapse of a flexible homopolymer may proceed through a combination of sausage and pearl-necklace intermediates [29].

Focus of the existing studies, mostly using flexible homopolymers, was on extracting the scaling of the collapse time with the length of the polymer and growth kinetics of the “pearls” or clusters. In this regard, only recently an analogy has been drawn between this cluster growth with the usual coarsening phenomena in spin or particle system [30]. Consequently, various tools from the well-established field of coarsening phenomena have been successfully employed in understanding the collapse kinetics of a flexible homopolymer [15–19]. Even though this allowed numerical estimations of the scaling of the collapse time and cluster growth, a unified understanding for different classes of polymers (i.e., for semi-flexible polymers) based on pre-existing theoretical foundations is still lacking.

Cluster-cluster aggregation is the underlying mechanism of self-assembly across a range of length scale from cosmology [31] to intra-cellular organization [32]. In this regard, the work of Smoluchowski is the first to provide a mean-field theory of clustering [33]. Later, based on the seminal diffusion-limited aggregation model [34], more general mod-

[†] smajumder.@amity.edu, suman.jdv@gmail.com

^{*} saikat.chakraborty@univ-grenoble-alpes.fr

els for kinetics of cluster-cluster aggregation have been proposed [35, 36], which can effectively overcome the limitations of the mean-field description. In this context, Vicsek and Family [37] suggested that the cluster size distributions as a function of cluster size and time follow a universal dynamic scaling form [38–41]. This has been later verified in numerical systems exhibiting cluster-cluster aggregation. In particular, experiments on colloidal aggregates have established that the underlying scaling functions are universal, being independent of the chemical composition of the colloids [40, 42–44]. Apart from colloids, experiments in externally driven ferrofluids, cellular organelles, or surface aggregations can also be successfully described by the theory [32, 45, 46].

On the other hand, as already mentioned there have been multiple studies that indicate the presence of cluster-cluster aggregation during the collapse of a polymer. In spite of that, to the best of our knowledge, no effort has been dedicated to apply the Vicsek-Family scaling principles in understanding the same. The necessity of such an approach, advocating universality in cluster sizes is increasingly becoming important as conformational changes in complex bio-macromolecule like proteins require better understanding of the underlying principles of polymer physics. To this end, here, by means molecular dynamics (MD) simulations we investigate the kinetics of collapse of homopolymers, ranging from flexible to moderately stiff ones (semiflexible), with an emphasis on exploring the presence of any dynamic scaling, as found in colloidal systems.

The rest of the paper is organized in the following manner. Next, in Sec. II we introduce the model polymer and details of the performed MD simulations. Following that in Sec. III we provide a brief description of the existing scaling theory for particle systems, and thereby introduce the observables which we calculate. In Sec. IV we present the simulation results. Finally, we present summary and discussions in Sec. V.

II. MODEL AND METHODS

We consider a coarse-grained bead-spring model polymer chain consisting of N monomers or beads of mass m and diameter σ , connected in a linear fashion. The bond between successive monomers, which are at a distance r apart is realized via the standard finitely extensible non-linear elastic (FENE) potential [47]

$$V_{\text{FENE}}(r) = -\frac{1}{2}KR_0^2 \ln \left[1 - \left(\frac{r}{R_0} \right)^2 \right]; \quad r < R_0, \quad (1)$$

where we chose the spring constant $K = 30\epsilon/\sigma^2$ and $R_0 = 1.5\sigma$. The monomers also interact with each other via the standard Lennard-Jones (LJ) potential

$$V_{\text{LJ}}(r) = 4\epsilon \left[\left(\frac{\sigma}{r} \right)^{12} - \left(\frac{\sigma}{r} \right)^6 \right], \quad (2)$$

with the interaction strength ϵ . The repulsive part in V_{LJ} takes care of the volume exclusion of the monomers and the attractive part ensures a collapse transition for the polymer as

a function of temperature. For convenience the LJ potential is truncated, shifted and force corrected at $r_c = 2.5\sigma$, leading to

$$V_{\text{LJ}}^{\text{mod}}(r) = \begin{cases} V_{\text{LJ}}(r) - V_{\text{LJ}}(r_c) - (r - r_c) \frac{dV_{\text{LJ}}}{dr} \Big|_{r=r_c} & r < r_c, \\ 0 & \text{otherwise.} \end{cases} \quad (3)$$

The modified potential behaves qualitative the same as V_{LJ} , however, is continuous and differentiable at $r = r_c$. The energy penalty for bending of the polymer backbone is given by

$$V_{\text{bend}} = \kappa \sum_{i=1}^{N-2} (1 - \cos \theta_i), \quad (4)$$

where θ_i is the angle between consecutive bonds and κ is the bending stiffness. The case of $\kappa = 0$ stands for a flexible polymer with no bending energy penalty and $\kappa > 0$ corresponds to a semiflexible polymer. The described model exhibits a collapse transition as a function of temperature where at high temperature the polymer attains an extended coil conformation and at low temperature it remains as a compact conformation.

We perform MD simulations of the above model. The equation of motions of the polymer beads are solved using the standard velocity-Verlet integration scheme [48]. The temperature is kept constant using the Nosé-Hoover chain thermostat [49–51]. The discrete time step of integration is chosen to be $\Delta t = 5 \times 10^{-4} \tau_0$, where $\tau_0 = \sqrt{m\sigma^2/\epsilon}$ is the standard LJ unit of time. The unit of temperature T is ϵ/k_B . For convenience, in our simulations we set m , σ and ϵ to unity. For faster computation we rely on the simulation package LAMMPS [52].

Since we study the nonequilibrium dynamics of the collapse transition of a polymer, an extended-coil conformation of a polymer is desired as the initial configuration. For that we use a self-avoiding walk of length $N - 1$ as a polymer with N monomers. Using this self-avoiding walk we perform MD simulation at a high T for an extended period such that polymer chain attains an extended-coil conformation. Following that we start the nonequilibrium evolution by setting $T = 1$. We present results for polymers with three different chain lengths, $N = 512, 1024$ and 2048 . As we are interested in the kinetics of collapse transition, here, we present result for polymer with moderate bending stiffness, i.e., $\kappa \in [0, 10]$. For even larger κ , the collapse transition accompanies with other complex conformational transitions [53]. Except the evolution snapshots and contact maps all data presented are averaged over 300 independent realizations obtained by using different seed for the random number while generating the self-avoiding walk.

III. DYNAMIC SCALING THEORY

Before we move forward to the simulation results, here, we briefly discuss the dynamic scaling theory pertinent to understand cluster-cluster aggregation during colloidal self assembly. During the course of this discussion we also introduce

various relevant quantities that will be used later. Here, by a cluster of size s we refer to the number of particles (or monomers) forming the cluster. In our cluster identification method, an aggregate of monomers with s beyond a threshold $s_c = 10$ is considered to be a cluster [19]. Thus, if $N_s(t)$ is the number of clusters of size s at time t , the total number of clusters is

$$n_c(t) = \sum_{s=10} N_s(t), \quad (5)$$

and the average size of the clusters

$$C_s(t) = \frac{\sum_s s N_s(t)}{n_c(t)}. \quad (6)$$

Typically, cluster-cluster aggregation occurs via a power-law growth as

$$C_s(t) \sim t^z, \quad (7)$$

where z is the corresponding growth exponent. The dynamic scaling theory relates the cluster size distribution to their time evolution through the expression [37]

$$N_s(t) \sim s^{-2} f\left(\frac{s}{t^z}\right). \quad (8)$$

The scaling function $f(x)$ exhibits a power-law behavior for $x \ll 1$: $f(x) \sim x^\delta$, where δ is the crossover exponent. For very large x , one gets $f(x) \ll 1$. Thus, at a fixed t when $s \ll C_s(t)$, one expects a power-law dependence of $N_s(t)$ on s and t as

$$N_s(t) \sim s^{-\tau} t^{-w}, \quad (9)$$

with $w = z\delta$ and $\tau = 2 - \delta$. This leads to the scaling relation

$$w = (2 - \tau)z. \quad (10)$$

Alternatively, $N_s(t)$ may have a different relation with s and t , given as [54]

$$N_s(t) \sim s^{-2} \tilde{f}\left(\frac{s}{t^z}\right), \quad (11)$$

where $\tilde{f} = x^2 g(x)$ is a different scaling function. The cut-off function $g(x)$ describes a fast decay for both $x \gg 1$ and $\ll 1$. In this case, $N_s(t)$ will have bell-shaped profiles. Thus, rewriting the s and t dependence similar to Eq. (9), one arrives at a different scaling relation given by

$$w = 2z. \quad (12)$$

The dynamic scaling theory was generalized [54] by showing its dependence on the diffusion of the clusters. The diffusion constant D_s of cluster of size s scales as

$$D_s \sim s^\gamma, \quad (13)$$

where the exponent γ decides the type scaling relation. The generalized theory predicts that for $\gamma > \gamma_c$ the relation (10) is valid and for $\gamma < \gamma_c$ one expects Eq. (12) to be applicable.

Here, γ_c is a critical value below which aggregation dynamics is dominated only by the large cluster–small cluster interactions, and above which large-small and large-large clusters processes contribute equally. Thus, combining the two cases one can write down a general scaling relation

$$w = z\delta, \quad (14)$$

where the crossover exponent δ is given by

$$\delta = \begin{cases} (2 - \tau) & \text{for } \gamma > \gamma_c \\ 2 & \text{for } \gamma < \gamma_c. \end{cases} \quad (15)$$

IV. RESULTS

A. Flexible polymers

We begin by showing representative conformations of a flexible polymer illustrating the time evolution during its collapse, in Fig. 1. Starting from an extended-coil-like conformation, at early times, clusters of monomers or “pearls” develop randomly along the chain. Such developments result in appearance of locally dense regions. To identify these clustered regions on the chain, we estimate the inter-monomer pairwise distances for non-bonded monomers. We consider a pair of monomers to be in *contact*, if their distance is less than 2.5σ . On the two-dimensional contact maps, the colored diagonal corresponds to self contacts. These are almost the only contacts present at early times as shown in the first frame. Transient proximity of different segments of the fluctuating polymer generates the sporadic off-diagonal contacts. The developments of clusters with time appear as few off-diagonal contacts. The second and the third frame depict such intermediate stage of collapse representing the “pearl-necklace”. Visual inspection of the snapshot as the collapse progresses suggests decreased number of clusters, but with increased sizes. Consistent with the prediction of the pearl-necklace representation of the collapse, inspection of the trajectories reveal that the nucleated clusters merge with each other forming larger clusters. The corresponding contact map demonstrates this growth by increase in size of regions of off-diagonal or long-range contacts at the expense of their number. Finally, a single globule is formed after aggregation of all the clusters (final frame in Fig. 1), resulting in appearance of contacts throughout the chain.

To quantify these stages of collapse, we present the time evolution of the average number of clusters $\langle n_c \rangle$ for three different chain lengths in Fig. 2. Here and later $\langle \dots \rangle$ indicates averaging over different simulation runs performed using independent initial conformations. Following the temperature quench, clusters nucleate fast, resulting in an almost instantaneous rise of $\langle n_c \rangle$. Afterwards, for a short time period spanning up to about $t = 10$, the profiles remain almost flat. The plots are shifted upwards for longer polymers. A simultaneous inspection of the snapshots and contact maps in Figure 1 suggests that the clusters continue to grow during this time

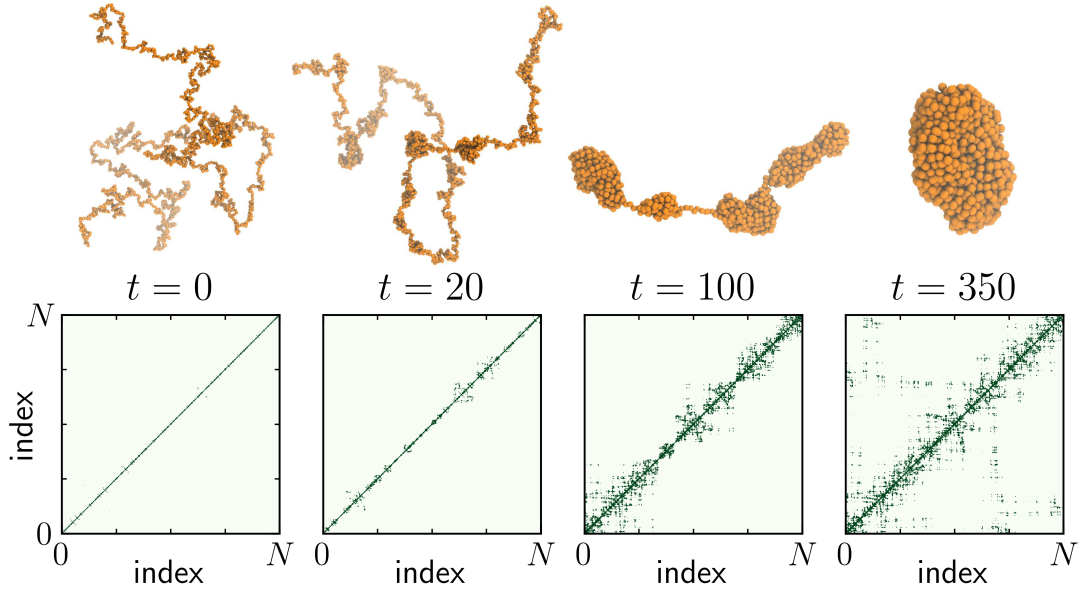


FIG. 1. Collapse of a flexible polymer. Representative snapshots at different times and their corresponding contact maps illustrating the sequence of events during the collapse of a flexible polymer of length $N = 2048$. The first frame shows the nucleation of small clusters or “pearl” along the polymer chain, indicated by development of monomer-monomer contacts (dark blue region). The second and third frames reflect growth of clusters with long (contour) distance contacts. The final frame represents the globular state with contacts spanning the whole chain.

window. Clearly, at this stage the growth occurs by acquiring monomers from the chains connecting the clusters, having no

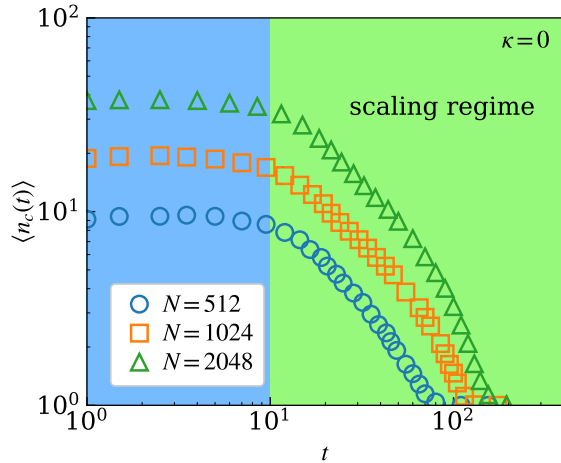


FIG. 2. Cluster-cluster aggregation in flexible polymers. Time evolution of the average number of clusters $\langle n_c \rangle$ for three different chain lengths. Profiles of $\langle n_c \rangle$ show a plateau at early times (blue background) followed by a monotonic decay (green background), consistent with the pear-necklace phenomenological picture.

impact on the number of clusters. The time span up to this stage appears to be independent of N . A monotonic decay to unity or a collapsed globule state follows the plateau. Evidently, aggregation of smaller clusters result in such decrease of $\langle n_c \rangle$. As expected, the formation of globule takes longer for larger N . Here, we focus on the spatio-temporal scales, where $\langle n_c \rangle$ undergoes the monotonic decay at intermediate to late stages of the collapse, and identify this cluster-cluster aggregation dominated stage as our regime of interest.

After identifying the time regime of interest, we explore whether the dynamic scaling in Eq. (8) or (11) can be extended to aggregations of clusters of monomers under the topological constraint of a polymer chain. As the first step, we check the variation of the average cluster size with time following Eq. (6) [see Fig. 3(a)]. The rise of $\langle C_s(t) \rangle$ for different N follow similar profiles, barring the saturation at late times. Such deviations are due to effects of finite lengths of the polymer chains. The preceding similarity suggests presence of identical kinetics of growth. The sluggish growth of $\langle n_c(t) \rangle$ for small t ($\lesssim 10$) is a signature of monomer acquisition by the existing clusters or “pearls”. This stage is followed by a faster growth which exhibits a linear behavior on the double-log scale, consistent with a power-law behavior in Eq. (7) with $z = 1.65$. A comparison of time scales between Figs. 2 and 3(a) confirms that the time period when $\langle C_s(t) \rangle$ shows increase is indeed the cluster-cluster aggregation regime, i.e.,

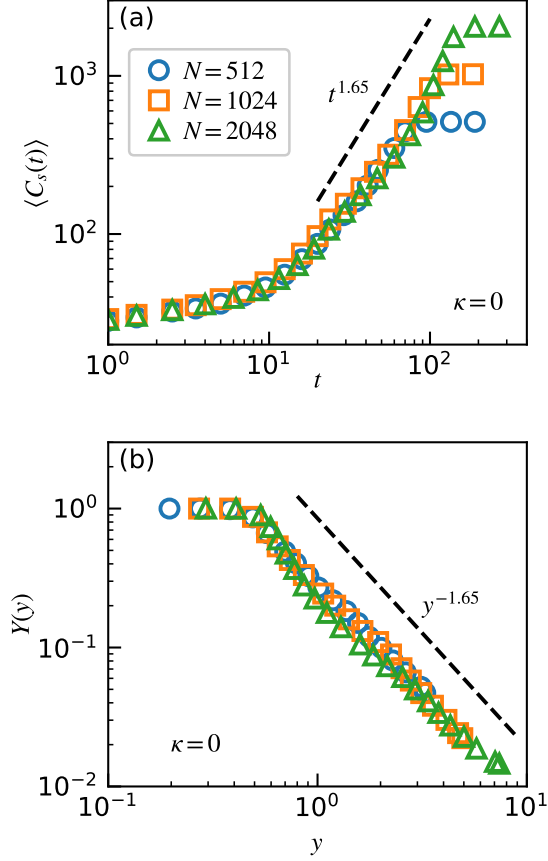


FIG. 3. Cluster growth in flexible polymers. (a) Growth of the average cluster size $\langle C_s(t) \rangle$ during the collapse of polymers of three different lengths N . The dashed line shows the consistency of the data with a power-law growth with an exponent $z = 1.65$. (b) Plots of the scaling functions $Y(y)$, demonstrating the collapse of data for different N through a finite-size scaling analysis providing an unambiguous estimate of z . In both (a) and (b) the data are shown on a double-log scale.

our regime of interest.

To obtain an unambiguous estimate of z , we account for the finite-size effects by constructing a finite-size scaling analysis [16, 55, 56]. For that we write down the following growth ansatz

$$\langle C_s(t) \rangle = C_0 + A_z t^z, \quad (16)$$

where C_0 corresponds to the initial offset. To account for the finite-size effect we introduce a finite-size scaling function $Y(y)$ such that

$$Y(y) = \frac{\langle C_s(t) \rangle - C_0}{N - C_0}. \quad (17)$$

For the choice of the scaling variable

$$y = \frac{\langle C_s \rangle - C_0}{N - C_0}, \quad (18)$$

in this exercise by tuning the value z , one thus expects that the data for different N to collapse onto each other for the

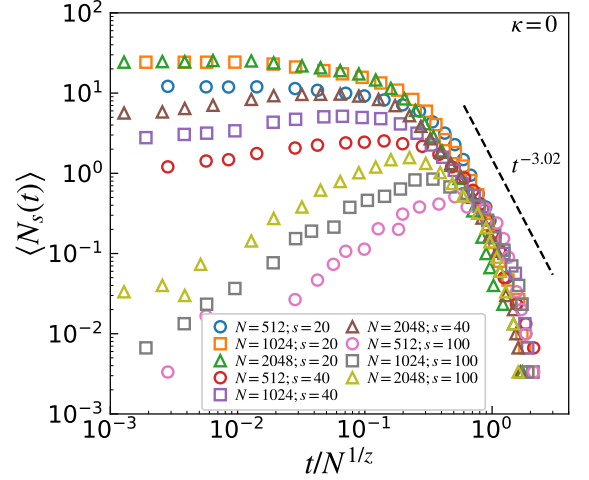


FIG. 4. Kinetics of clusters of fixed sizes in flexible polymers. Time dependence of the number N_s of clusters of fixed size s on a double-log scale, during the collapse. Plots for multiple s across different N are included. The abscissa is scaled with $N^{1/z}$ for a better visualization. $N_s(t)$ display both monotonic and bell-shaped profiles.

appropriate choice of z along with a $Y(y) \sim y^{-z}$ behavior in the finite-size unaffected regime. The optimum result of this exercise is demonstrated in Fig. 3(b) that confirms the value of $z \approx 1.65$.

Next, we measure the variation in the number of clusters $N_s(t)$ of a fixed size s with time, shown in Fig. 4. We choose the values of $s \geq 20$, which belong to the scaling regime in $\langle C_s(t) \rangle$ [see Fig. 3(a)]. The plots include results from three different N to distinctly identify the finite-size unaffected regime. The t axis is scaled with $N^{1/z}$ to facilitate

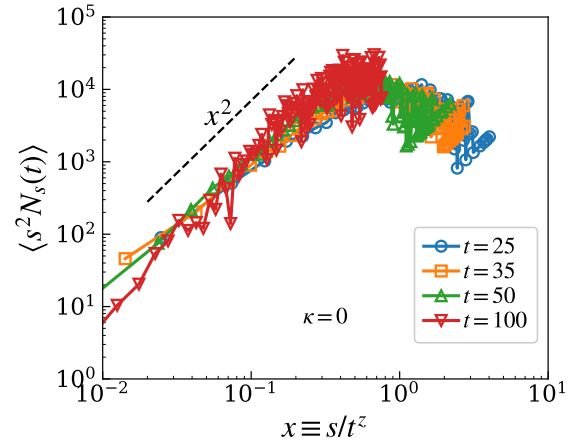


FIG. 5. Verification of dynamic scaling in a flexible polymer. Double-log plots of the scaling function $f(x) \equiv s^2 N_s(t)$ against the scaling variable $x \equiv s/t^z$ at different times for a polymer of length $N = 2048$. The dashed black line shows the consistency of the data with the power law $\sim x^2$ in the regime $x \ll 1$. Collapse of data at different times confirms the presence of colloid-like dynamic scaling during flexible polymer collapse.

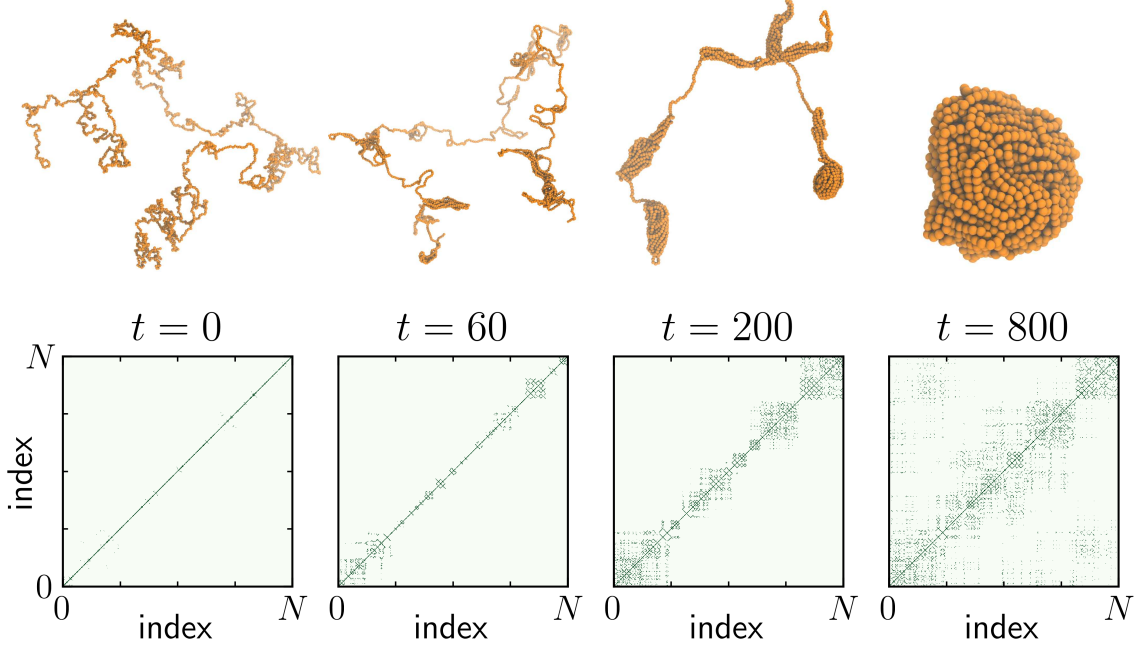


FIG. 6. Collapse of a semiflexible polymer. Representative time evolution snapshots at four different times and their corresponding contact maps during the collapse of a semi-flexible polymer with a bending stiffness $\kappa = 8$ and chain length $N = 2048$.

a better visualization of data for different N . At early times, mostly small clusters are present. Whereas, clusters with large s appear later at the expense of the smaller ones. Thus, $N_s(t)$ for smaller s starts the decay from a higher value. Also, their decay are concurrent with the rise in the number of larger clusters. In the intermediate to late times, data for different s across different N collapse on a power-law decay function. Keeping in mind Eq. (9), in this regime we fit the expression

$$N_s(t) = A_w t^{-w}, \quad (19)$$

which yields $w \approx 3.02 \pm 0.12$.

Having both z and w in hand, we move on to investigate the distribution of cluster sizes for different times in the scaling regime and check if there exists any Viscek-Family-like dynamic scaling. For that in Fig. 5 we present the scaling function $f(x) \equiv s^2 N_s(t)$ as a function of the scaling variable $x \equiv s/t^z$ for different t using data for a polymer with $N = 2048$. The data for different t show a reasonable data collapse. The data in the regime $x \ll 1$ show an increase consistent with the power law $\sim x^2$ as shown by the solid line, which indicates that possibly $\tau = 0$. Thus one can expect that the validity of the scaling relation Eq. (12). Recalling $z = 1.65(3)$ and $w = 3.12(12)$, it can be inferred that within numerical error for flexible polymer indeed that is the case. Overall, we conclude that colloid-like dynamic scaling for cluster-cluster aggregation can also be realized in case of clusters composed of monomers during collapse of a flexible polymer.

B. Semi-flexible polymers

Though pearl-necklace model describes the pathways during the collapse of a semiflexible polymer as well, the local structures of the monomer clusters are known to be different from the flexible polymers [57]. Local structures can potentially determine the shape of the clusters on polymer, which in turn can alter the kinetics of cluster aggregation. Since, we use polymers having moderate κ values, it is ensured that the final conformation will still be a globule [53, 58], however, the dynamics of collapse could still have lot of variations [29].

Representative evolution snapshots and corresponding contact maps during the collapse of a semiflexible polymer with a reasonably high value of bending stiffness $\kappa = 8$ are presented in Fig. 6. At early times, there is development of clusters, leading to few contacts close to the diagonal. This is followed by aggregation of the small clusters forming of larger regions of off-diagonal contacts. Eventually, a globule is formed where long-range contacts are present over the whole chain. The progressions are similar to those in flexible polymers. However, significantly more order with diamond-like moieties can be noticed in the contact maps for the semi-flexible case. Such order has been reported earlier, and the diamond-like structures in contact maps have been attributed to the ordered local structures for semi-flexible polymers [57].

Having an idea about the phenomenology of cluster-cluster aggregation during collapse of semiflexible polymers, we

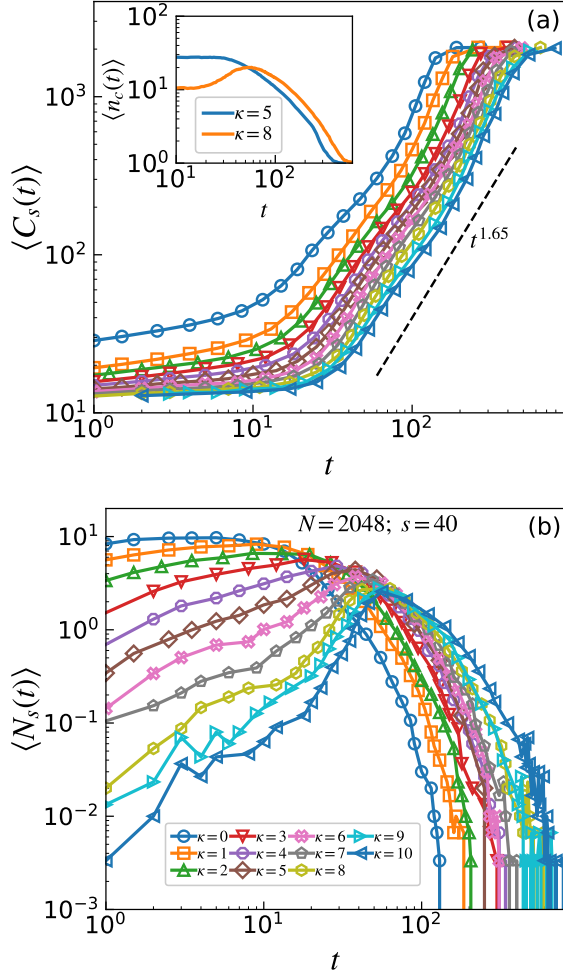


FIG. 7. Cluster growth in semiflexible polymers. (a) Plot of $C_s(t)$ on a double-log scale for different κ for a polymer with $N = 2048$. The dashed line represents a power law as indicated. Note that the case $\kappa = 0$ represents a flexible polymer. The inset shows the time dependence of the average number of clusters $\langle n_c(t) \rangle$ for two different κ . (b) Corresponding plots of the time dependence of the number of clusters $\langle N_s(t) \rangle$ of fixed size $s = 40$.

move on to quantify the cluster growth as a function of time. Corresponding plots for different κ for a fixed chain length $N = 2048$ are presented in Fig. 7(a). As in the case of flexible polymers, $\langle C_s(t) \rangle$ for all κ display a relatively slow rise at early time, followed by a power-law growth in the scaling regime. As κ increases the entry into the scaling regime gets delayed. This can be further confirmed from corresponding plots for time dependence of the number of clusters $n_c(t)$ for $\kappa = 5$ and $\kappa = 8$, presented in the inset of Fig. 7(a). There, the non-monotonic profile for $\kappa = 8$ appears because of the time-independent size cut-off, $s_c = 10$ used to identify the clusters. If one compares the data for the cluster growth for different κ , it appears that in the scaling regime they are almost parallel to each other, implying the presence of a universal growth exponent z , irrespective of κ . Nevertheless, we fit the ansatz in Eq. (16) to the data, results of which are compiled in Table I.

The results yield no systematic dependence of the estimated z values on κ . Rather it fluctuates around a mean $z = 1.65$. Of course, to further confirm the presence of a κ -independent z , one can rely on finite-size scaling analysis of individual κ , as done for the flexible case in the previous subsection. However, for the sake of brevity, here, we do not present such exercises for different κ .

To obtain the exponent w , we probe the time dependence of $N_s(t)$, i.e., by calculating the variations in the count of clusters of size s with time. Representative plots for $N = 2048$ and $s = 40$ is presented in Fig. 7(b). As κ increases one notices a progressively prominent bell-shaped non-monotonic behavior for the same value of s . This is due to the fact that with increasing κ nucleation of clusters to form stable clusters gets delayed, as also evident from plots of number of clusters $\langle n_c(t) \rangle$ in the inset of Fig. 7(a). For each considered κ , we fit the region with a common decay for different s (not shown here) to the expression in Eq. (19). The obtained estimates of w are quoted in Table II. The value of w appears to decrease with increasing κ . Also, the value of w becomes smaller than $2z$ as the polymer becomes stiffer. This suggests deviation from the scaling relation in of Eq. (12). The deviations motivate us to ask whether the dynamic scaling at all exists for semi-flexible polymers. If yes, then possibly the cluster-cluster aggregation in semiflexible polymer can be represented by the other kind of dynamic scaling functional form as embedded in Eqs. (8) and (10).

Particularly for the scaling relation in Eq. (10), the exponent τ corresponding to the cluster size distribution becomes important. To extract the exponent, as in flexible polymer (see Fig. 5), we first verify if the dynamic scaling holds in semi-flexible polymers as well by using the data for cluster-size distributions at different times during the collapse. Our exercise reveals that indeed the dynamic scaling holds for semiflexible polymers. In Figs. 8(a) and (b) we illustrate this finding for two κ values for a polymer of length $N = 2048$. There the plots of the scaling function $f(x) \equiv \langle s^2 N_s(t) \rangle$ at different times as a function of the scaling variable $x \equiv s/t^z$ show reasonably good data collapse for both κ . For other values of κ as well we obtain such data collapse. Note that the times used in (a) and (b) are different because as κ increases the entry to the scaling regime gets delayed, as already discussed. In fact, for

TABLE I. Fitting of the ansatz in Eq. (16) to the data for time dependence of the cluster size for polymers with different stiffness κ .

κ	C_0	A_z	z	t -range
0	32.54(10)	0.37(1)	1.65(3)	[1 : 140]
1	18.65(44)	0.22(1)	1.66(2)	[1 : 140]
2	15.05(10)	0.20(2)	1.61(2)	[1 : 150]
3	12.93(52)	0.16(2)	1.60(2)	[1 : 200]
4	8.56(10)	0.12(2)	1.63(3)	[20 : 300]
5	6.97(50)	0.10(1)	1.66(3)	[20 : 300]
6	4.80(20)	0.08(8)	1.67(1)	[30 : 320]
7	3.07(20)	0.07(1)	1.68(2)	[30 : 340]
8	3.27(10)	0.05(1)	1.69(3)	[30 : 340]
9	3.20(20)	0.05(2)	1.63(2)	[30 : 360]
10	3.10(20)	0.03(3)	1.61(3)	[30 : 360]

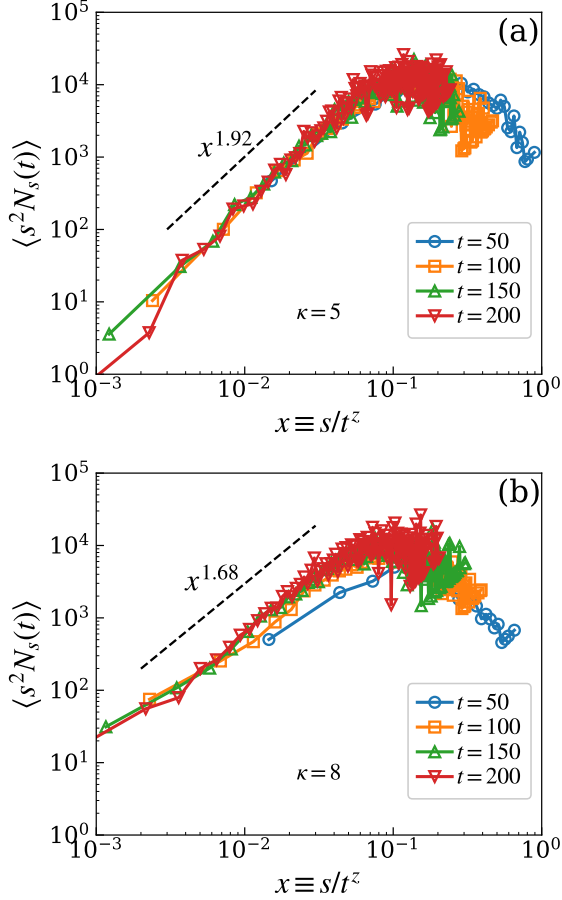


FIG. 8. Verification of dynamic scaling in semiflexible polymers. Double-log plot of the scaling function $f(x) \equiv \langle s^2 N_s(t) \rangle$ against the scaling variable $x \equiv s/t^z$ at different times for a polymer of length $N = 2048$ with bending stiffness (a) $\kappa = 5$ and (b) $\kappa = 8$. The dashed black lines show the consistency of the data with the power law $\sim x^\delta$ in the regime $x \ll 1$, with respective values of δ as indicated. Collapse of data at different times confirm the presence of colloid-like dynamic scaling in semiflexible polymers.

TABLE II. Fitting of the ansatz in Eq. (19) to the data for decay of the number of cluster of a fixed size s as a function of time for polymers with fixed $N = 2048$ and different κ .

κ	$A_w(10^4)$	w	range
0	8.14(37)	3.02(12)	[30, 150]
1	4.39(93)	3.21(6)	[30, 150]
2	2.70(77)	2.98(7)	[50, 250]
3	2.07(57)	2.70(6)	[30, 100]
4	38.68(57)	2.87(9)	[50, 200]
5	52.35(75)	2.88(5)	[50, 200]
6	32.92(90)	2.70(10)	[50, 200]
7	7.44(85)	2.28(8)	[50, 200]
8	4.96(10)	2.08(9)	[80, 300]
9	7.93(76)	2.07(9)	[80, 300]
10	3.32(98)	1.82(10)	[100, 400]

$\kappa = 8$ one can notice that the data for $t = 50$ and 100 are a bit off for the same reason. In the region $s/t^z \ll 1$, the data show

TABLE III. Fitting of Eq. (20) to the data of the scaling function $f(x)$ as a function of the scaling variable x at different times for polymers with fixed length $N = 2048$ and different κ .

κ	$A_\delta(10^5)$	δ
0	2.18(37)	2.20(25)
1	4.50(17)	2.12(18)
2	3.30(77)	2.21(21)
3	2.53(57)	2.16(17)
4	3.07(33)	2.11(13)
5	17.33(75)	1.92(20)
6	16.56(90)	1.83(10)
7	13.01(85)	1.71(8)
8	13.26(10)	1.68(10)
9	5.20(26)	1.52(10)
10	5.96(28)	1.54(12)

a power-law behavior with an expected exponent $\delta = 2 - \tau$, as discussed earlier. We observe consistent behavior in this regime, and extract δ and thereby τ from these plots by doing a fit using a power law

$$f(x) = A_\delta x^\delta, \quad (20)$$

in this regime. The results from the fitting exercise are quoted in Table III. The results indicate that δ decreases monotonically as a function of κ , i.e., τ increases monotonically with κ . Now, recalling the estimated values of z and w , reveals that as κ increases one deviates from the relation in Eq. (12). The deviation can be quantified by Δ as a function of κ , where

$$\Delta = \frac{w}{2z} \quad (21)$$

is a measure of the deviation from scaling relations in Eq. (12). The corresponding plots as a function of κ is presented in Fig.

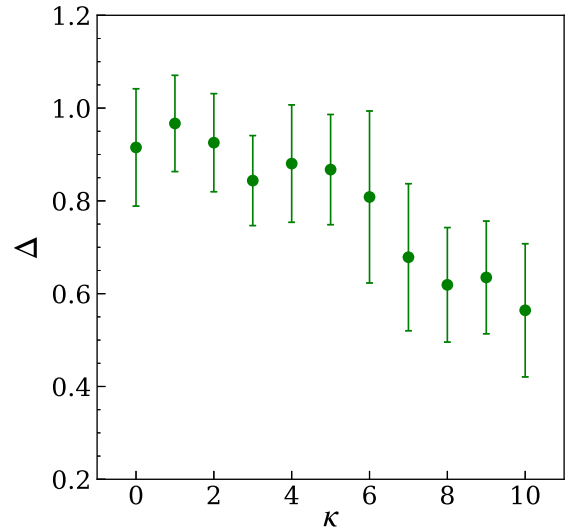


FIG. 9. Deviation from the Viscek-Family-like scaling. Plot of Δ accounting the deviation from scaling relations in Eq. (12) as a function of the bending stiffness for a polymer of length $N = 2048$.

9. The data clearly depict that for small κ the scaling relation in Eq. (12) holds true with $\Delta \approx 1$ and for $\kappa \geq 5$ it does not hold anymore. We have also checked the deviation from Eq. (10), however, there we do not find any meaningful trend.

In cluster-cluster aggregation of purely particle systems, the validity of the scaling functions in Eqs. (8) or (11) depends on how the clusters diffuse before they coalesce with each other [54]. The diffusion constant of cluster of depends on the size s as described in Eq. (13). As already pointed out, there exists a critical value of the exponent γ_c , such that for $\gamma > \gamma_c$ one realizes the scaling relation in Eq. (10) and for $\gamma < \gamma_c$ the relation in Eq. (12) holds true. In the present case, as in most of realistic situations, obviously $\gamma < 0$, which indicates that D_s should decrease with increasing s . In addition, our results for small κ value also suggests that they belong to the scenario of $\gamma < \gamma_c$. To dig further about the deviation of the data from the scaling relation for $\kappa \geq 5$, one can rely on a comparative analyses of the diffusion constant D_s as a function of κ .

For estimating the D_s one needs to monitor a cluster of reasonably large size, and from its trajectories needs to calculate mean-squared displacement of the center of mass of the cluster. However, during the collapse of a polymer the clusters formed are not sufficiently long lived to have a trajectory that can provide a reasonable estimate of D_s . Hence, we opt for an indirect comparison of D_s for different κ . We recall that the local structures in semiflexible polymers are more order than those in a flexible polymer. Differences in order may lead to changes in shape. Thus, a cluster of size s can have different hydrodynamic or Stokes-Einstein radius R_h , depending on the stiffness of the polymer, resulting in variation in effective diffusion coefficient as $D_s \sim 1/R_h$.

To test the hypothesis, we estimate R_h of clusters of fixed size $s \approx 100$ and 200, which represent cluster sizes well within the scaling regime for all κ . For the calculation, we use the simplified Kirkwood approximation given as [25, 59–61]

$$\frac{1}{R_h} = \frac{1}{s} \sum_{i=1}^s \sum_{j=1, j \neq i}^s \left\langle \frac{1}{d_{ij}} \right\rangle, \quad (22)$$

where $d_{ij} = |\vec{r}_i - \vec{r}_j|$ is the distance between any two monomers i and j within the cluster of size s . Note that here $\langle \dots \rangle$ represents averaging over different clusters. Along the same line we also calculate the radius of gyration of the cluster as

$$R_g = \sqrt{\frac{1}{2s^2} \sum_{i,j} (\vec{r}_i - \vec{r}_j)^2}. \quad (23)$$

The ratio of R_h and R_g gives a comparative idea about the shapes of the clusters of same size. The variation of R_h with κ is shown in in Fig. 10(a) for the two values of s . The profiles show a marginal dip around $\kappa = 2$ following which it increases steadily. This suggests that clusters of same size will be more elongated and loosely bound as κ increases, as also revealed from the typical clusters of size $s \approx 200$ for a small and large κ . Similarly, in Fig. 10(c) the ratio R_h/R_g indicate a change in shape of the clusters around $\kappa \approx 5$. Smaller

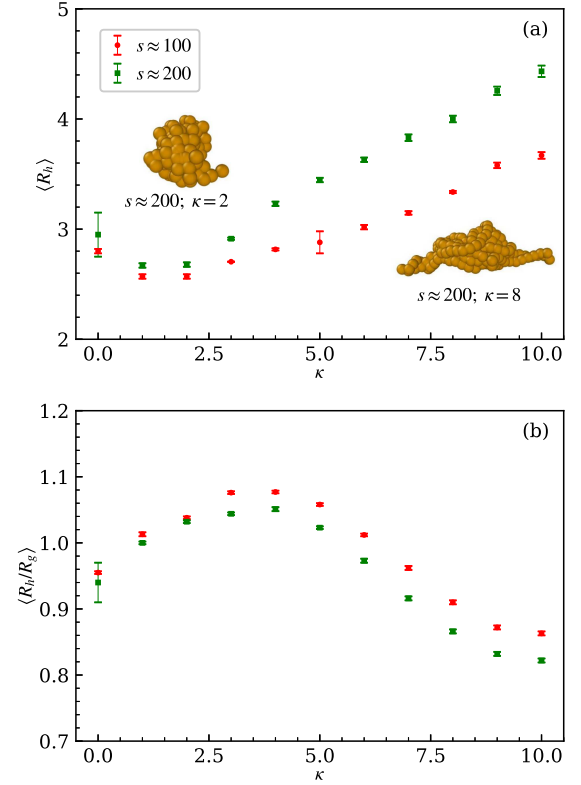


FIG. 10. Hydrodynamic radius of clusters. (a) Average hydrodynamic radius $\langle R_h \rangle$ of clusters as a function of κ for two different choices of cluster sizes $\langle s \rangle$ for a polymer of length $N = 2048$. The snapshots represent typical clusters of size $\langle s \rangle \approx 200$ obtained at a small and a large κ , as indicated. (b) Corresponding variation of the ratio $\langle R_h/R_g \rangle$, where R_g is the radius of gyration of the cluster.

value of the ratio indicates a smaller fractal dimensions of the clusters with increasing κ . This the behavior of the data in Fig. 10 strongly implies a change in the diffusion constant D_s with κ . A comparison with Fig. 9 confirms that the deviation from the scaling relation in Eq. (12) onsets around the same value of κ . Since the scaling relation in Eq. (12) is based on the diffusion of the clusters and its dependence on its size, this correlation is certainly strong. Here, we confirm that indeed there is a change in the diffusion of the clusters at around the same value of κ where Eq. (12) breaks down. Of course, a detailed theoretical treatment of this correlation is needed to further substantiate it.

V. DISCUSSION

We have investigated the collapse kinetics for a range of homopolymers from flexible to moderately stiff ones, using MD simulations at constant temperature of a bead-spring model. Following a quench from an extended coil-like conformation to a temperature below the collapse transition we have monitored the trajectory of the polymer until it becomes a globule. The nonequilibrium pathway of the collapse more or less

follows the popular pearl-necklace picture, irrespective of the bending stiffness κ . The intermediate to late stage of the pathway is dominated by the aggregation of “pearls” or clusters of monomers. Drawing analogies with the cluster formation during colloidal assembly, here, we have aimed to verify the existence of associated dynamic scaling of cluster-cluster aggregation during polymer collapse.

The verification was performed by measuring the time dependence of the average cluster size $C_s(t)$, time dependence of the number of cluster of fixed size $N_s(t)$ and the cluster-size distribution at different times. Our results for the cluster growth indicates a universal power-law behavior $C_s(t) \sim t^z$ with $z \approx 1.65$, irrespective of κ . However, the exponent w associated with the long-time decay $N_s(t) \sim t^{-w}$, varies inversely with κ . Interestingly, distributions of cluster sizes exhibit the dynamic scaling of the form $N_s(t) \sim s^{-2} f(s/t^z)$, irrespective of κ . Otherwise difficult to estimate from our data, the realization of this scaling also allowed us to calculate the the exponent τ associated with the cluster-size distribution at a fixed time as $N_s \sim s^{-\tau}$. From the estimated values of z , w and τ we have discovered that for small $\kappa < 5$, in addition to the dynamic scaling, the relation $w = 2z$ is also obeyed. For $\kappa \geq 5$ the estimated exponents show systematic deviation from the relation as a function of κ . This suggests that even though presence of dynamic scaling can be realized during polymer collapse, irrespective of the bending stiffness, the nature of scaling varies in terms of the relation between the dynamic exponents.

The dynamic scaling, observed here for polymers is routinely observed for a wide range of colloidal aggregations. There, observation of a specific kind of scaling function is determined by factors such as size dependent diffusion constant of the clusters. In polymers, larger κ lead to higher local order and different shape of the clusters compared to flexible or weakly stiff polymers. Thus, to find the origin of the breakdown of the scaling relation for large κ in polymer collapse, we have estimated the hydrodynamic R_h of the “pearls” or clusters. For the same monomer count s , the clusters belonging to semiflexible polymers show larger R_h , implying a smaller effective diffusion coefficient. The κ -dependent profile of R_h follows the same trend as the scaling relation deviates from flexible polymers to semiflexible polymers. Thus, we speculate that the local order induced shape change as the cause of the change in the governing scaling law in cluster-cluster aggregation during polymer collapse.

Historically, tracking the collapse of single polymers experimentally was difficult due to technical challenges in generating ultra-dilute solutions or obtaining sufficiently long monodisperse polymers [3, 62]. Significant progress in addressing these issues have been achieved through high reso-

lution of modern instruments, e.g., small-angle X-ray scattering, single-molecule fluorescence, and dielectric spectroscopy have enabled probing of conformational changes in individual macromolecule with time [21, 63–66]. However, validation of the dynamic scaling behavior observed in this work would require well-resolved visualization of the intermediate states with clusters along the chain. While time-resolved investigations of colloidal aggregation and peptide assembly are now routinely performed [67–70], capturing the rapid collapse dynamics of polymers remains challenging due to spatio-temporal limitations of the conventional imaging techniques such as bright-field, confocal, time-resolved atomic force, or cryogenic transmission electron microscopy (cryo-TEM). Notably, the collapse time is expected to scale with polymer length as $\tau_c \sim N^\nu$, where typically $\nu = 1 - 2$ [19]. Thus, recent advances in synthesis of ultra-high-molecular-weight polymers have the potential to extend collapse times to the scale of hours [71–73]. Additionally, viscosity and temperature of the ambient solvent can be tuned to prolong the collapse time [16, 29]. Under such conditions and in sufficiently dilute solutions, cryo-TEM may become a viable technique for imaging and quantifying the size distribution of intermediate clusters at various time points [69, 74]. Although such experimental efforts would require substantial resources and optimization, we anticipate that continued progress in polymer synthesis and imaging technologies will soon enable the direct observation of these transient collapse intermediates.

For colloids, these scaling principles are known to be universal, independent of the composition of colloids [40, 41]. The observation of similar principles in polymer expands the domain of the universality of these theories. The analogies with colloidal aggregations further reaffirms the validity of droplet coalescence model of polymer collapse. As a next step, it would be worth to verify the same for collapse of heteropolymers or protein-like heteropolymers. A step even further would be to perform all-atom MD simulations of polypeptide collapse and check the universality of the dynamic scaling. In this regard, one can also investigate the collapse of a real globular protein.

ACKNOWLEDGMENTS

The work was funded by the Anusandhan National Research Foundation (ANRF), Govt. of India through a Ramanujan Fellowship (File no. RJF/2021/000044). The authors thank Aritra Sarkar for useful discussions on the experimental methods.

-
- [1] P. J. Flory, *Principles of polymer chemistry* (Cornell university press, 1953).
 - [2] W. H. Stockmayer, “Problems of the statistical thermodynamics of dilute polymer solutions,” *Macromol. Chem. Phys.* **35**, 54–74 (1960).

- [3] I. Nishio, S.-T. Sun, G. Swislow, and T. Tanaka, “First observation of the coil-globule transition in a single polymer chain.” *Nature* **281**, 208–209 (1979).
- [4] P.-G. de Gennes, “Kinetics of collapse for a flexible coil,” *J. Phys. Lett.* **46**, 639–642 (1985).

- [5] A. Byrne, P. Kiernan, D. Green, and K. A. Dawson, “Kinetics of homopolymer collapse,” *J. Chem. Phys.* **102**, 573 (1995).
- [6] E. G. Timoshenko, Y. A. Kuznetsov, and K. A. Dawson, “Kinetics at the collapse transition: Gaussian self-consistent approach,” *J. Chem. Phys.* **102**, 1816–1823 (1995).
- [7] Y. A. Kuznetsov, E. G. Timoshenko, and K. A. Dawson, “Kinetics at the collapse transition of homopolymers and random copolymers,” *J. Chem. Phys.* **103**, 4807–4818 (1995).
- [8] Y. A. Kuznetsov, E. G. Timoshenko, and K. A. Dawson, “Kinetic laws at the collapse transition of a homopolymer,” *J. Chem. Phys.* **104**, 3338–3347 (1996).
- [9] Y. A. Kuznetsov, E. G. Timoshenko, and K. A. Dawson, “Equilibrium and kinetic phenomena in a stiff homopolymer and possible applications to DNA,” *J. Chem. Phys.* **105**, 7116–7134 (1996).
- [10] L. I. Klushin, “Kinetics of a homopolymer collapse: Beyond the rouse–zimm scaling,” *J. Chem. Phys.* **108**, 7917–7920 (1998).
- [11] N. Kikuchi, J. F. Ryder, C. M. Pooley, and J. M. Yeomans, “Kinetics of the polymer collapse transition: The role of hydrodynamics,” *Phys. Rev. E* **71**, 061804 (2005).
- [12] X. Ye, Y. Lu, L. Shen, Y. Ding, S. Liu, G. Zhang, and C. Wu, “How many stages in the coil-to-globule transition of linear homopolymer chains in a dilute solution?” *Macromolecules* **40**, 4750–4752 (2007).
- [13] T. T. Pham, M. Bajaj, and J. R. Prakash, “Brownian dynamics simulation of polymer collapse in a poor solvent: Influence of implicit hydrodynamic interactions,” *Soft Matter* **4**, 1196–1207 (2008).
- [14] J. Guo, H. Liang, and Z.-G. Wang, “Coil-to-globule transition by dissipative particle dynamics simulation,” *J. Chem. Phys.* **134**, 244904 (2011).
- [15] S. Majumder and W. Janke, “Cluster coarsening during polymer collapse: Finite-size scaling analysis,” *Europhys. Lett.* **110**, 58001 (2015).
- [16] S. Majumder, J. Zierenberg, and W. Janke, “Kinetics of polymer collapse: Effect of temperature on cluster growth and aging,” *Soft Matter* **13**, 1276 (2017).
- [17] H. Christiansen, S. Majumder, and W. Janke, “Coarsening and aging of lattice polymers: Influence of bond fluctuations,” *J. Chem. Phys.* **147**, 094902 (2017).
- [18] S. Majumder, U. H. E. Hansmann, and W. Janke, “Pearl-necklace-like local ordering drives polypeptide collapse,” *Macromolecules* **52**, 5491–5498 (2019).
- [19] S. Majumder, H. Christiansen, and W. Janke, “Understanding nonequilibrium scaling laws governing collapse of a polymer,” *Euro. Phys. J. B* **93**, 142 (2020).
- [20] S. J. Hagen and W. A. Eaton, “Two-state expansion and collapse of a polypeptide,” *J. Mol. Biol.* **301**, 1019–1027 (2000).
- [21] M. Sadqi, L. J. Lapidus, and V. Muñoz, “How fast is protein hydrophobic collapse?” *Proc. Natl. Acad. Sci. U.S.A.* **100**, 12117 (2003).
- [22] G. Haran, “How, when and why proteins collapse: The relation to folding,” *Curr. Opin. Struct. Bio.* **22**, 14–20 (2012).
- [23] J. B. Udgaonkar, “Polypeptide chain collapse and protein folding,” *Arch. Biochem. Biophys.* **531**, 24–33 (2013).
- [24] G. Reddy and D. Thirumalai, “Collapse precedes folding in denaturant-dependent assembly of ubiquitin,” *J. Phys. Chem. B* **121**, 995 (2017).
- [25] S. Chakraborty, T. I. Morozova, and J.-L. Barrat, “Intrinsically disordered proteins can behave as different polymers across their conformational ensemble,” *J. Phys. Chem. B* **129**, 2359–2369 (2025).
- [26] X. Zeng, K. M. Ruff, and R. V. Pappu, “Competing interactions give rise to two-state behavior and switch-like transitions in charge-rich intrinsically disordered proteins,” *Proc. Natl. Acad. Sci. U.S.A.* **119**, e2200559119 (2022).
- [27] A. Halperin and Paul M. Goldbart, “Early stages of homopolymer collapse,” *Phys. Rev. E* **61**, 565–573 (2000).
- [28] J. Xu, Z. Zhu, S. Luo, C. Wu, and S. Liu, “First Observation of Two-stage Collapsing Kinetics of a Single Synthetic Polymer Chain,” *Phys. Rev. Lett.* **96**, 027802 (2006).
- [29] S. Majumder, H. Christiansen, and W. Janke, “Temperature and viscosity tune the intermediates during the collapse of a polymer,” *Macromolecules* **57**, 10586–10599 (2024).
- [30] A. J. Bray, “Theory of phase-ordering kinetics,” *Adv. Phys.* **43**, 357–459 (1994).
- [31] S. W. Hawking, I. G. Moss, and J. M. Stewart, “Bubble collisions in the very early universe,” *Phys. Rev. D* **26**, 2681 (1982).
- [32] D. S. W. Lee, C.-H. Choi, D. W. Sanders, L. Beckers, J. A. Riback, C. P. Brangwynne, and N. S. Wingreen, “Size distributions of intracellular condensates reflect competition between coalescence and nucleation,” *Nat. Phys.* **19**, 586–596 (2023).
- [33] M. von Smoluchowski, “Brownsche molekularbewegung und koagulation von kolloidteilchen,” *Z. Phys.* **17**, 585–599 (1916).
- [34] T. A. Witten Jr and L. M. Sander, “Diffusion-limited aggregation, a kinetic critical phenomenon,” *Phys. Rev. Lett.* **47**, 1400 (1981).
- [35] P. Meakin, “Formation of fractal clusters and networks by irreversible diffusion-limited aggregation,” *Phys. Rev. Lett.* **51**, 1119 (1983).
- [36] M. Kolb, R. Botet, and R. Jullien, “Scaling of kinetically growing clusters,” *Phys. Rev. Lett.* **51**, 1123 (1983).
- [37] T. Vicsek and F. Family, “Dynamic scaling for aggregation of clusters,” *Phys. Rev. Lett.* **52**, 1669–1672 (1984).
- [38] F. Family, P. Meakin, and T. Vicsek, “Cluster size distribution in chemically controlled cluster–cluster aggregation,” *J. Chem. Phys.* **83**, 4144–4150 (1985).
- [39] S. Miyazima, P. Meakin, and F. Family, “Aggregation of oriented anisotropic particles,” *Phys. Rev. A* **36**, 1421 (1987).
- [40] M. Y. Lin, H. M. Lindsay, D. A. Weitz, R. C. Ball, R. Klein, and P. Meakin, “Universality in colloid aggregation,” *Nature* **339**, 360–362 (1989).
- [41] M. Y. Lin, H. M. Lindsay, D. A. Weitz, R. C. B. R. Klein, R. C. Ball, and P. Meakin, “Universal diffusion-limited colloid aggregation,” *J. Phys.: Condens. Matt.* **2**, 3093 (1990).
- [42] D. A. Weitz, J. S. Huang, M. Y. Lin, and J. Sung, “Dynamics of diffusion-limited kinetic aggregation,” *Phys. Rev. Lett.* **53**, 1657 (1984).
- [43] D. A. Weitz and M. Y. Lin, “Dynamic scaling of cluster-mass distributions in kinetic colloid aggregation,” *Phys. Rev. Lett.* **57**, 2037 (1986).
- [44] N. E. Valadez-Pérez, Y. Liu, and R. Castañeda-Priego, “Reversible aggregation and colloidal cluster morphology: the importance of the extended law of corresponding states,” *Phys. Rev. Lett.* **120**, 248004 (2018).
- [45] J. Černák, G. Helgesen, and A. T. Skjeltorp, “Aggregation dynamics of nonmagnetic particles in a ferrofluid,” *Phys. Rev. E* **70**, 031504 (2004).
- [46] K. Shahriver, E. Carreón-González, J. R. Morillas, and J. de Vicente, “Aggregation kinetics of carbonyl iron based magnetic suspensions in 2d,” *Soft Matter* **13**, 2677–2685 (2017).
- [47] K. Kremer and G. S. Grest, “Dynamics of entangled linear polymer melts: A molecular-dynamics simulation,” *J. Chem. Phys.* **92**, 5057–5086 (1990).
- [48] D. Frenkel and B. Smit, *Understanding Molecular Simulations: From Algorithms to Applications* (2002).
- [49] S. Nosé, “A unified formulation of the constant temperature molecular dynamics methods,” *J. Chem. Phys.* **81**, 511–519

- (1984).
- [50] W. G. Hoover, “Canonical dynamics: Equilibrium phase-space distributions,” *Phys. Rev. A* **31**, 1695 (1985).
 - [51] G. J. Martyna, M. L. Klein, and M. Tuckerman, “Nosé–Hoover chains: The canonical ensemble via continuous dynamics,” *J. Chem. Phys.* **97**, 2635–2643 (1992).
 - [52] S. Plimpton, “Fast parallel algorithms for short-range molecular dynamics,” *J. Comput. Phys.* **117**, 1–19 (1995).
 - [53] S. Majumder, M. Marenz, S. Paul, and W. Janke, “Knots are generic stable phases in semiflexible polymers,” *Macromolecules* **54**, 5321–5334 (2021).
 - [54] P. Meakin and F. Vicsek, T. and Family, “Dynamic cluster-size distribution in cluster-cluster aggregation: Effects of cluster diffusivity,” *Phys. Rev. B* **31**, 564–569 (1985).
 - [55] S. Majumder, S. K. Das, and W. Janke, “Universal finite-size scaling function for kinetics of phase separation in mixtures with varying number of components,” *Phys. Rev. E* **98**, 042142 (2018).
 - [56] J. Schneider, M. K. Meinel, H. Dittmar, and F. Müller-Plathe, “Different stages of polymer-chain collapse following solvent quenching—scaling relations from dissipative particle dynamics simulations,” *Macromolecules* **53**, 8889–8900 (2020).
 - [57] A. Lappala and E. M. Terentjev, “Raindrop coalescence of polymer chains during coil–globule transition,” *Macromolecules* **46**, 1239–1247 (2013).
 - [58] D. T. Seaton, S. Schnabel, D. P. Landau, and M. Bachmann, “From flexible to stiff: Systematic analysis of structural phases for single semiflexible polymers,” *Phys. Rev. Lett.* **110**, 028103 (2013).
 - [59] J. G. Kirkwood, “The general theory of irreversible processes in solutions of macromolecules,” *J. Polym. Sci.* **12**, 1–14 (1954).
 - [60] B. Liu and B. Dünweg, “Translational diffusion of polymer chains with excluded volume and hydrodynamic interactions by brownian dynamics simulation,” *J. Chem. Phys.* **118**, 8061–8072 (2003).
 - [61] F. Pesce, E. A. Newcombe, P. Seiffert, E. E. Tranchant, J. G. Olsen, C. R. Grace, B. B. Kragelund, and K. Lindorff-Larsen, “Assessment of models for calculating the hydrodynamic radius of intrinsically disordered proteins,” *Biophys. J.* **122**, 310–321 (2023).
 - [62] B. Chu, Q. Ying, and A. Y. Grosberg, “Two-stage kinetics of single-chain collapse. polystyrene in cyclohexane,” *Macromolecules* **28**, 180–189 (1995).
 - [63] L. Pollack, M. W. Tate, A. C. Finnefrock, C. Kalidas, S. Trotter, N. C. Darnton, L. Lurio, R. H. Austin, C. A. Batt, S. M. Gruner, and S. G. J. Mochrie, “Time resolved collapse of a folding protein observed with small angle x-ray scattering,” *Phys. Rev. Lett.* **86**, 4962–4965 (2001).
 - [64] M. Tress, E. U. Mapesa, W. Kossack, W. K. Kipnusu, M. Reiche, and F. Kremer, “Glassy dynamics in condensed isolated polymer chains,” *Science* **341**, 1371–1374 (2013).
 - [65] H. Hofmann, A. Soranno, A. Borgia, K. Gast, D. Nettels, and B. Schuler, “Polymer scaling laws of unfolded and intrinsically disordered proteins quantified with single-molecule spectroscopy,” *Proc. Nat. Acad. Sci. U. S. A.* **109**, 16155–16160 (2012).
 - [66] S. Naudi-Fabra, M. Tengo, M. R. Jensen, M. Blackledge, and S. Milles, “Quantitative description of intrinsically disordered proteins using single-molecule fret, nmr, and saxs,” *J. Am. Chem. Soc.* **143**, 20109–20121 (2021).
 - [67] D. Grober, I. Palaia, M. C. Uçar, E. Hannezo, A. Šarić, and J. Palacci, “Unconventional colloidal aggregation in chiral bacterial baths,” *Nat. Phys.* **19**, 1680–1688 (2023).
 - [68] L. Wu, C. P. Ortiz, and D. J. Jerolmack, “Aggregation of elongated colloids in water,” *Langmuir* **33**, 622–629 (2017).
 - [69] C. J. Newcomb, T. J. Moyer, S. S. Lee, and S. I. Stupp, “Advances in cryogenic transmission electron microscopy for the characterization of dynamic self-assembling nanostructures,” *Curr. Opin. Colloid Interface Sci.* **17**, 350–359 (2012).
 - [70] S. Chakraborty, C. M. Berac, B. Kemper, P. Besenius, and T. Speck, “Modeling supramolecular polymerization: The role of steric effects and hydrophobic interactions,” *Macromolecules* **52**, 7661–7667 (2019).
 - [71] H. Gao, “Synthesis of linear polymers in high molecular weights via reaction-enhanced reactivity of intermediates using friedel–crafts polycondensation,” *ACS Omega* **6**, 4527–4533 (2021).
 - [72] Y.-T. Chou, W.-R. Lee, and S.-S. Yu, “Efficient synthesis of ultrahigh molecular weight poly(methyl methacrylate) via visible light-induced raft polymerization in deep eutectic solvent,” *Macromolecules* **57**, 9241–9249 (2024).
 - [73] C. B. Eades, K. C. Stevens, D. E. Cabrera, M. K. Vereb, M. E. Lott, J. I. Bowman, and B. S. Sumerlin, “Ultra-high molecular weight polymer synthesis via aqueous dispersion polymerization,” *Chem. Sci.* **16**, 5573–5578 (2025).
 - [74] J. P. Patterson, Y. Xu, M.-A. Moradi, Nico A. J. M. Sommerdijk, and H. Friedrich, “Cryotom as an advanced analytical tool for materials chemists,” *Acc. Chem. Res.* **50**, 1495–1501 (2017).